Pergamon

Geochimica et Cosmochimica Acta, Vol. 68, No. 3, pp. 491–502, 2004

0016-7037/04 $30.00 + .00

doi:10.1016/S0016-7037(00)00482-4

Geochemical evolution of highly alkaline and saline tank waste plumes during seepage through vadose zone sediments

JIAMIN WAN,[1,*] TETSU K. TOKUNAGA,[1] JOERN T. LARSEN,[1] and R. JEFF SERNE[2]

[1]Earth Sciences Division, Lawrence Berkeley National Laboratory, Berkeley, CA 94720, USA
[2]Environmental Technology Division Pacific Northwest National Laboratory, Richland, WA 99352, USA

(*Received April* 3, 2003; *accepted in revised form July* 7, 2003)

Abstract—Leakage of highly saline and alkaline radioactive waste from storage tanks into underlying sediments is a serious environmental problem at the Hanford Site in Washington State. This study focuses on geochemical evolution of tank waste plumes resulting from interactions between the waste solution and sediment. A synthetic tank waste solution was infused into unsaturated Hanford sediment columns (0.2, 0.6, and 2 m) maintained at 70°C to simulate the field contamination process. Spatially and temporally resolved geochemical profiles of the waste plume were obtained. Thorough OH^- neutralization (from an initial pH 14 down to 6.3) was observed. Three broad zones of pore solutions were identified to categorize the dominant geochemical reactions: the silicate dissolution zone (pH $>$ 10), pH-neutralized zone (pH 10 to 6.5), and displaced native sediment pore water (pH 6.5 to 8). Elevated concentrations of Si, Fe, and K in plume fluids and their depleted concentrations in plume sediments reflected dissolution of primary minerals within the silicate dissolution zone. The very high Na concentrations in the waste solution resulted in rapid and complete cation exchange, reflected in high concentrations of Ca and Mg at the plume front. The plume-sediment profiles also showed deposition of hydrated solids and carbonates. Fair correspondence was obtained between these results and analyses of field borehole samples from a waste plume at the Hanford Site. Results of this study provide a well-defined framework for understanding waste plumes in the more complex field setting and for understanding geochemical factors controlling transport of contaminant species carried in waste solutions that leaked from single-shell storage tanks in the past.

1. INTRODUCTION

The Hanford Site, located in southeastern Washington, was one of the United States Department of Energy's major nuclear weapons production facilities from 1940 to 1989 (Riley et al., 1992). About 2×10^5 m^3 of high-level radioactive and hazardous wastes are stored in 177 underground tanks, including 149 single-shell tanks located in the 200 East and West Areas at the center of the Hanford Site. Over time, 67 of the single-shell tanks have leaked or are suspected of having leaked. About 2300 to 3400 m^3 of tank waste solution leaked between the 1950s and 1970s, releasing uranium, cesium, strontium, tritium, technetium, iodine, plutonium, chromium, and nitrates (DOE, 1996). Contaminants such as ^{137}Cs, ^{99}Tc, U, Cr(VI) and nitrates have been found in elevated concentrations in the vadose zone and all but ^{137}Cs have been found in groundwater beneath the single-shell tank farms (Ward et al., 1997; CH2M HILL, 2001; McKinley et al., 2001; Zachara et al., 2002). The U.S. Department of Energy has ongoing projects at the Hanford Site to monitor existing contaminant plumes in groundwater and to characterize the subsurface distribution of contaminants in tank farms that have impacted groundwater and sediments. These efforts include the Tank Farm Vadose Zone Characterization Project and the 200 Area Remedial Action Project.

Site characterization activities provide the basis for corrective and remedial action decisions. These activities identify scientific questions for resolution through research, and have included collection of many subsurface samples exhibiting varying degrees of contamination and physical/chemical changes. Although much has been learned concerning waste migration, the combination of subsurface heterogeneity and the limitations of field borehole drilling prevent comprehensive, high-resolution inventories of the various contaminants. While a number of laboratory-based studies have made considerable progress toward understanding reactions between tank waste solutions and Hanford sediments, the integration of laboratory and field understanding remains a challenge. Several factors contribute to the gap between field-based observations and many laboratory findings. Most laboratory studies, focused on specific interactions, employ batch equilibration approaches that, in principle, occur somewhere within the contaminated region. However, such approaches by themselves cannot generally identify where within a contaminant plume their isolated reactions are important. Linking such laboratory results to field applications is made even more difficult when recalling that only very small fractions of contaminant plumes are typically sampled or otherwise characterized. The research presented here aims to bridge this gap between field processes and laboratory experiments. We developed a laboratory column-profiling method that permits measurements that have direct correspondence to field contaminant plumes. Besides directly integrating geochemical reactions and transport processes, the method permits direct sampling of pore solutions and sediments within a waste plume with high spatial and temporal resolution. Using this approach, we studied the Hanford SX tank waste-leakage problem, and compared our laboratory results with the geochemical data recently obtained from the field site characterization project.

The focus of this study is on evolution of geochemical

* Author to whom correspondence should be addressed (jwan@lbl.gov).

Table 1. Major chemical components of SXT waste solutions.

Element	Our simulated TWS (molar)	Historical composition of SX-111 (molar)[a]	Historical composition of SX-108 (molar)[a]	Agnew's estimate (molar) [a]
Al	0.805	0.805	1.7	0.7 to 1.9
Cl	—	—	0.25	0.09 to 0.26
CO_3	0.168	0.168	—	0.2 to 0.3
F	0.014	0.014	—	—
OH	1.47	1.47	1.52	3 to 8.5
NO_3	4.72	4.72	8.14	2.3 to 6.3
NO_2	0.84	0.84	0.45	1 to 2.9
PO_4	0.0055	0.0055	—	0.04 to 0.12
SO_4	0.06	0.06	0.01	0.1 to 0.3
Na	8.05	8.05	10.52	5 to 14
Si	0.0015	0.0015	—	—
Density	1.37 Mg m^{-3}		—	—
Viscosity	2.0 mPa s		—	—
pH	14		14	—

[a] Data from Agnew (1996) and Serne et al. (1998).

composition of a waste plume caused by interactions between the major ions (as opposed to the trace contaminants) of the waste solution and sediments. We believe that the behavior of trace elements can be understood only after understanding how the major geochemical conditions of a plume, especially pH, evolve as the plume grows.

2. MATERIALS AND METHODS

2.1. Sediment

The sediment used in the columns is the Hanford Formation "coarse sand," a glaciofluvial sediment collected from the 200 East Area of the Hanford Site. The 200 Areas are the principal waste management areas at Hanford and houses high-level waste tanks. The Hanford formation comprises ~85% of the vadose zone below the 200 Areas. The sand facies are mostly coarse to medium and contain scattered well-rounded pebbles and cobbles, with some thin discontinuous silt lenses (Swanson et al., 1988). The major components are feldspar, quartz, and basaltic rock fragments (Serne et al., 1998; Reidel et al., 1999; Serne et al., 2002a). The sediment used in our study contains 93% sand, 6.0% silt, and 1.0% clay. The median grain-size is 350 μm, and average grain density is 2.77 Mg m^{-3}. Calcium carbonate comprises 1.1% of the total mass. The pH of water extract was 8.4 (water to soil mass ratio = 1:1, at 21°C for 24 h).

2.2. Simulated Tank Waste Solution (TWS)

The chemical composition of our simulated TWS (Table 1) is based on the historical composition of the SX-111 tank waste. The composition of the SX-108 tank waste, also included in Table 1, will be discussed later. We choose the SX-111 solution because, first of all, its composition is based on direct measurements. It is one of the few available data sets from historical chemical analyses of tank supernatant solutions. Second, the data are well within the range of the estimates of Agnew et al. (1996) of SX tank supernatant solutions. Third, the solution is stable at room temperature, and easy to handle in the laboratory. The major ions in our simulated TWS include 0.8 mol/L Al^{3+}, 8 mol/L Na^+, 5 mol/L NO_3^-, with a pH of 14. All added salts were completely dissolved within hours of stirring at room temperature. The solution was filtered (0.45 μm) before use.

2.3. Column and Column-Sectioning Method

Each experiment was conducted by infusing simulated tank waste solution into a sediment column (Fig. 1). Three different column lengths (0.23, 0.55, and 2.05 m) were used to simulate a waste plume

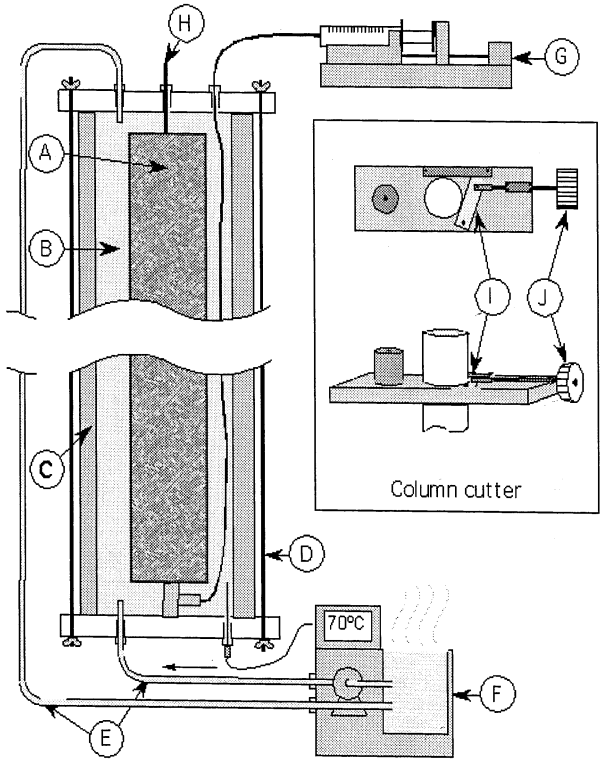

A Sediment-filled Teflon column
B Hot-water-filled Lexan column
C Insulation
D Threaded retaining rod
E Hot-water circulation tubes
F Temperature-regulating water bath
G Syringe pump
H Sediment column outlet
I Cutting blade
J Blade advancing knob

Fig. 1. Schematic diagram of the section-column and column-cutter.

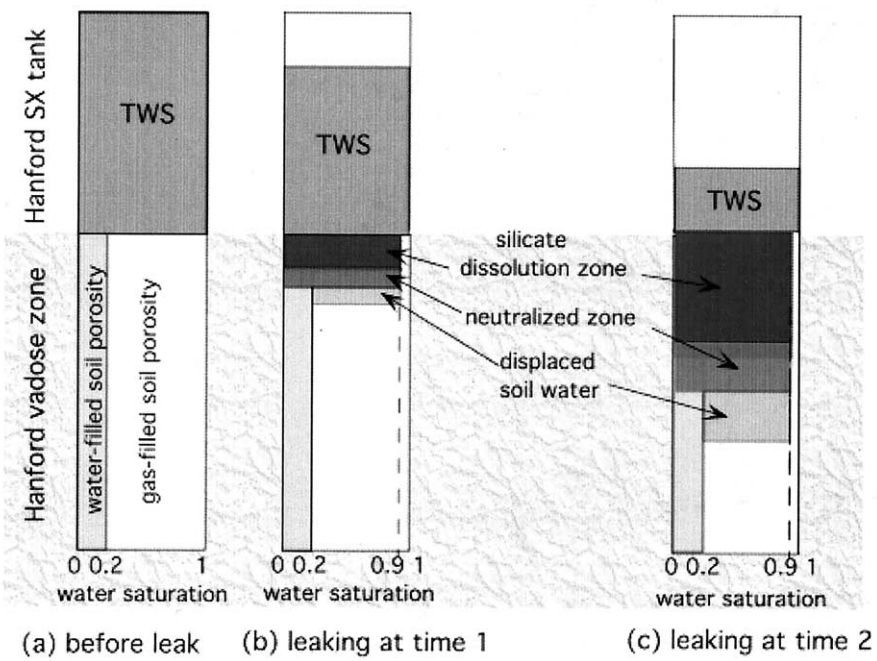

Fig. 2. Conceptual profiles of tank waste-plume evolution.

at different stages. Hanford sediment with 5.4% mass initial moisture was homogeneously packed to an equivalent dry bulk density of 1.65 Mg m^{-3} into the inner column (Teflon, 38 mm I.D., 5.3 mm wall thickness, variable length). After packing, the sediment column was inserted into an outer column (Lexan, 82 mm I.D., 3.2 mm wall thickness) that provided temperature control through connection with a recirculating temperature-regulating water bath. The outside of the water-bath column was wrapped with insulation to minimize heat loss. Since heating from radioactive decay resulted in self-boiling within SX waste tanks and elevated temperatures in the surrounding contaminated sediments, the experiments were conducted with the temperature maintained at 70 ± 1.0°C. The TWS was injected into the sediment column using a syringe pump, at a pore-water velocity of 100 mm d^{-1}. Lacking information on actual tank leak rates, this somewhat arbitrary flow rate corresponds to a plume migration of ~37 m in 1 yr. To avoid gravity-induced flow fingering, we injected the fluid from the bottom of the vertical column. Therefore, each column was nearly saturated at the time outflow occurred. When effluent (displaced native soil water) was first detected at the outlet, injection was terminated and the column was immediately sectioned.

In sectioning the column, the top lid of the water-bath column was removed and a column cutter was attached to the top of this column. The column cutter had a blade mounted on top of an aluminum plate, and a hole in the center machined to fit around the sediment column. The blade could be adjusted back and forth by turning a knurled knob. By rotating the assembly, the blade was pushed deeper into the Teflon wall until it cut through, and the column section could be removed. The sediment column was incrementally lifted from the water-bath column and was sectioned every few centimeters at desired intervals. Separating each column segment took ~60 s. Each separated section was placed immediately into a vacuum filter unit, made of polypropylene with a 0.45 μm pore-size, 50 mm diameter cellulose acetate membrane (Corning Inc. Acton, MA). The pore-solution sample was immediately vacuum-extracted from the sediment into a polypropylene centrifuge tube attached to the filter. The solutions extracted from different sections were analyzed for their pH, electrical conductivity (EC) and major cation composition. Sediment from each segment was analyzed for its major elemental composition. The resulting spatially resolved chemical analyses permitted reconstruction of waste-plume evolution.

2.4. Chemical Analysis Methods

usually direct pH measurements of highly alkaline solutions have not been accurate when using conventional glass electrodes or nonglass pH probes, because of the difficulty in standardizing the pH meters at pH values above 12.5. Therefore, in our study a Sentron IntelliProbe ISFET HotLine pH electrode was used in mV mode. Samples were measured for their mV values and their pH values were calculated based on a mV-pH standard calibration. The mV-pH standard curve was generated using commercially available pH standards: pH 4, 7, 10 (JT Baker Standards), and 12.45 (Oakton). For pH 13 and 14 standards, 0.1 N and 1 N NaOH solutions were made in our laboratory. The IntelliProbe was connected to a Fisher Scientific Model 15 pH Meter. Our estimated error for these measurements was ≤ 0.25 pH units. We also found that a Corning Semi-Micro combo glass pH electrode can be standardized at pH 12.45 and gives good readings up to pH 14. This electrode was connected to a Denver Instrument Model 225 pH/ISE meter. Although the systems of interest are elevated in temperature and ionic strength, our pH measurements were conducted at 25°C. Because of the complexity of these solutions, we did not attempt to calculate pH and OH^- concentrations in pore fluids during permeation by using temperature, activity, and dissociation constant corrections.

EC measurements were conducted on solutions that were diluted 100× with distilled water. This level of dilution provided EC values that were linearly correlated with sums of major ion concentrations. To determine the major element compositions of the extracted pore liquids, we used an ICP-OES (Thermo Jarell Ash Hi Res IRIS). Since many of these liquid extracts contained precipitates formed after the extraction, aqua regia, hydrofluoric acid, and boric acid were used to dissolve precipitates (Hossner, 1996). The sediment segments were analyzed at the X-ray Fluorescence Laboratory at the Washington University.

3. RESULTS AND DISCUSSION

3.1. Conceptual Delineation of Plume Regions

For the purpose of interpreting column data presented in the following subsections, it is useful to first conceptually introduce the general features of a TWS plume found in this study.

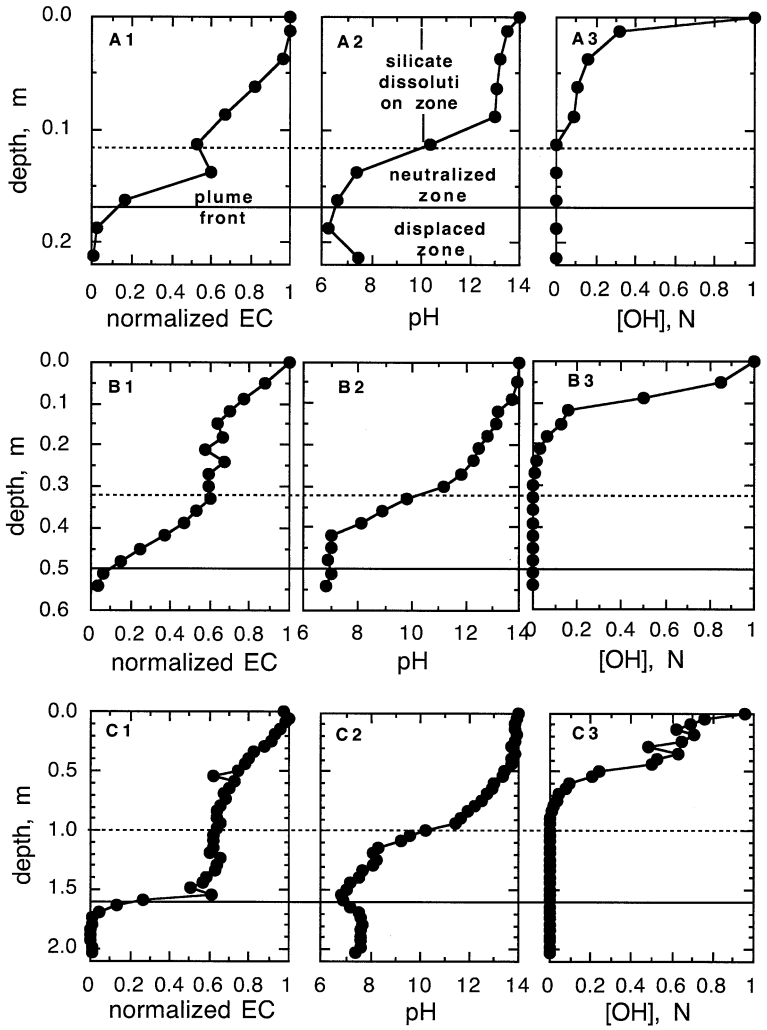

Fig. 3. EC, pH, and [OH^-] profiles along the 0.2, 0.6, and 2.0 m columns.

Figure 2a depicts the starting point, with a finite volume of TWS isolated from the underlying sediment of uniform initial moisture content. Figures 2b and 2c show conceptual profiles of the leaking TWS seepage into the sediment as plug flow, at progressive times. Moving from the uncontaminated sediment back toward the leaking source within a given profile, we defined three major zones based on distinctly different chemical compositions measured in their pore waters from the column results: (1) displaced native soil water zone, (2) a pH neutralized TWS zone, and (3) a silicate dissolution zone. All of these zones grow as more TWS leaks. Actual plumes will have more complex geometry and dispersion, but these diagrams illustrate the major characteristics expected along flow paths.

3.2. Evolution of Waste Plume pH and Salinity Profiles

The pore solutions extracted from individual sections within the 0.2, 0.6 and 2.0 m columns were analyzed for their salinity and pH. These salinity, pH, and OH^- (estimated from pH) profiles are presented in Figure 3. Recall that since ionic strength and activity corrections were not applied, the OH^- profiles are approximate. The distance axes in these figures are oriented to reflect the field geometry with downward migration of the contaminant (as in Fig. 2), rather than the upward flow imposed in the laboratory. Pore water salinity is presented in the left panels in terms of normalized EC. Normalized EC refers to the electrical conductivity of 100-times-diluted pore waters, relative to that of the initial TWS at the same dilution. The purpose of dilution is to ensure the linearity of EC measurements with respect to total ion concentrations. Moving downward from the TWS source within the plume, salinity and pH decline as the plume front is approached. The horizontal lines crossing all three panels denote the predicted plume front, calculated by assuming plug displacement by TWS with 95% saturation of the pore space. Salinity data show that this position is quite close to the inflection point of the normalized EC profiles. This plume front separates the displaced soil water zone and TWS plume zone. The displaced soil water zone contains primarily displaced initial soil water and is characterized by its normalized EC being close to zero and its pH being

close to 8. The displaced soil water zone also exhibits increasing influences from mixing with TWS as it approaches the plume front.

Dramatic pH reductions of the TWS at the plume front were measured, with pH reduced to as low as 6.3. The pH varied from 6.3 at the plume front to ~14 at the near-plume source (the middle panels in Fig. 3). Because of this very wide range in pH, and the related wide range in overall geochemistry, two broad zones within the waste plume were defined: the silicate dissolution zone and the neutralized zone. A pH of 10 was assigned to the boundary between the silicate dissolution zone (SDZ) and the neutralized zone (NZ). This boundary-defining pH was chosen based on the relatively low solubility of major silicates below this value. In addition, the original high OH^- concentration (≈1 mol/L) is largely depleted at pH equal to 10.

Defined by pH values greater than 10, the SDZ comprises the largest portion of the waste plume. Over the tested length scales, the SDZ extends about two-thirds of the distance of the plume. Within this zone, the pH monotonically decreases from 14, the value of the initial TWS. Primary silicate dissolution and zeolite precipitation have been reported as the dominant reactions when the highly alkaline and saline Hanford TWS reacted with the sediment (Wan et al., 2003; Bickmore et al., 2001). The OH^- concentration profile was estimated based on pH data and presented in the three right panels of Figure 3.

The high EC values of the NZ indicate that it still contains high concentrations of TWS and other ions dissolved or displaced (cation exchange) from the sediment. NZ pH values range from 6.3 to 10, and the length of this zone grows nearly in proportion to the length of the waste plume. Neutralized zones within the 0.2, 0.6, and 2.0 m columns are 32%, 36%, and 37% of the total plume length, respectively. General reactions responsible for pH neutralization are dissolution of primary silicates, and precipitation of some secondary minerals including calcite. The steps involved in neutralization of the TWS pH will be addressed in a separate study, and will not be discussed in any detail here.

A summary and comparison of the three columns of different lengths, with their different zones, are provided in Figure 4. Within the tested range, the SDZ and NZ both grow in approximately direct proportion to time and the volume of leaked TWS. This illustration provides the conceptual connection to the actual waste plumes in the Hanford Site. Details of the field plume will reflect different site-specific hydrogeochemical properties and their variability, as well as variable leakage history. Nevertheless, the neutralization features of the TWS plumes identified here are expected to occur in the field.

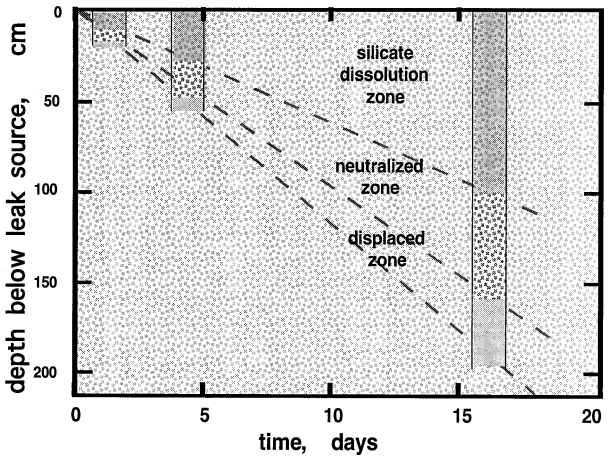

Fig. 4. Summary and comparison of three experimental columns of different lengths, showing zones of silicate dissolution, pH neutralization, and displaced soil water. Placement of the profiles along the time axis was determined by the TWS infusion time at which columns were sectioned.

3.3. Evolution of the Waste Plume Solution Chemistry

The pore solutions extracted from individual sections within the 0.6 and 2.0 m columns were analyzed for major cations to characterize the waste plume aqueous phase chemistry (Figs. 5 and 6, respectively). Data from the 0.2 m column are not available because of consumption of samples during early, unsuccessful analyses of solutions. As described previously, the plume front and the reaction zones in each column were identified based on injected TWS volume and pH. The solid horizontal lines denote the predicted location of the plume front, whereas the dashed lines divide the NZ and SDZ (located at pH = 10).

Since the influent TWS contained Na^+ at an extremely high concentration (8.05 mol/L, 185 g L^{-1}), this cation remained dominant in the waste-plume solution profile. Reactions involving Na^+ are cation exchange with Ca^{2+} and Mg^{2+} on the sediment's exchange sites, and precipitation in new phases, including amorphous sodium aluminosilicates, and sodium aluminum nitrate silicate hydrate, $Na_8Al_6SiO_{24}(NO_3)_2 \cdot 4H_2O$ (Wan et al., 2003). Through these processes, some Na^+ was lost from solution as the TWS seeped further into the sediment.

Sources of Al^{3+} in the pore liquids are from both the initial TWS and aluminosilicate dissolution. The measured Al^{3+} concentrations in pore solutions are very low, even within the high pH SDZ, recalling that the initially high Al^{3+} concentration (0.8 mol/L) in the TWS is stable in solution only at high pH, and precipitates as amorphous and crystalline $Al(OH)_3$ and other aluminosilicates when pH decreases and when reacting with the sediment. Even within the high pH SDZ, Al^{3+} was removed from the permeating TWS through precipitation with Si and formation of zeolites (Wan et al., 2003). Within the NZ, pH values are too low to sustain the elevated Al concentrations, resulting in rapid precipitation of Al hydroxides.

Iron is enriched in the pore solutions only at pH > 13. Based on our X-ray diffraction analyses, mineralogical analyses of Hanford sediments by others (McKinley et al., 2001; Serne et al., 2002a), and the kinetic study by Malstrom and Banwart (1997), biotite dissolution appears to be the likely source for aqueous Fe. Unlike many of the other common Fe-bearing minerals in these sediments (magnetite, pyroxene, olivine), biotite dissolution is favored under alkaline conditions.

Solution Si concentrations ranged between 0.3 to 0.9 mol/L within the highly alkaline SDZ. Based on the high-temperature solubility study of Rimstidt and Barnes (1980), these Si concentrations are under saturated with respect to amorphous silica throughout the SDZ, and even under saturated with respect to quartz within most of the SDZ. Beyond the SDZ, the dissolved

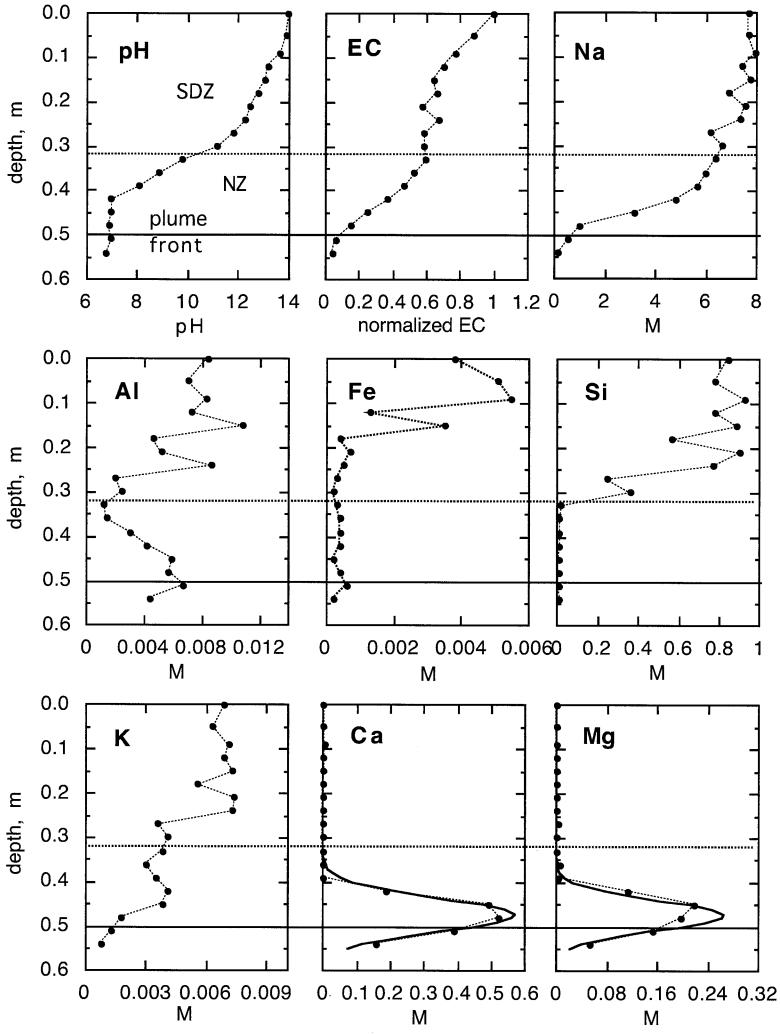

Fig. 5. Pore-water chemical-composition profiles within the 0.6 m column. The experiments were conducted at 70°C, and the waste-plume transport direction is plotted from top down. The smooth curves in the Ca and Mg plots are predications using displacement-dependent dispersion model.

Si concentrations decline substantially in response to solubility limits imposed by pH decreases.

The initial TWS did not contain K^+, and the enriched K^+ within the plume results from dissolution of K-containing minerals. Solubilities of orthoclase (Teng et al., 2001) and biotite mica (Malstrom and Banwart, 1997) both increase with increased pH and are likely sources for K^+ within the alkaline plume solution. The broadness of the regions with K^+-enriched solutions, as well as their clear lag behind the sharp Ca^{2+} and Mg^{2+} peaks, reflect that fact that kinetics of K^+ release are slow relative to simple cation exchange. Such slower release is consistent with mineral dissolution and gradual K^+ release from micas and feldspar.

Very sharp peaks of Ca^{2+} appear at the plume front, with values as high as 0.5 and 1.2 mol/L for the 0.6 and 2.0 m columns, respectively. Inventories of Ca^{2+} in these peak regions are equivalent to displacements of 46 and 49 $mmol_c$ (kg soil)$^{-1}$ within the waste plume, for the 0.6 and 2.0 m columns, respectively. For comparison, cation exchange capacity for coarser and finer Hanford sands reported by Serne et al. (2002a) ranged from 17 to 180 $mmol_c$ kg^{-1}. The common divalent cations Ca^{2+} and Mg^{2+} accounted for at least 79 and 13% of the exchangeable bases, respectively. Thus, the very high Ca^{2+} concentrations in the displacement front are within a range attributable to cation exchange with Na^+ in the TWS-permeated zones. The Ca^{2+} concentrations in the displaced front of the 0.6 m column are close to saturation with respect to calcite (system open to atmospheric CO_2). Higher Ca^{2+} concentrations in the displaced front of the 2.0 m column are above calcite solubility limits, indicating that calcite precipitation is occurring in this moving boundary region. Ca^{2+} in solution should be spatially distributed over a region that grows primarily through hydrodynamic dispersion. The shape of the exchange-displaced Ca^{2+} front in the 0.6 m column was fit to displacement-dependent dispersion, constrained to match the measured Ca^{2+} mass within the front. The dispersion coefficient was set equal to the pore solution velocity (0.10 m d^{-1}) times a dispersivity, which by minimizing root mean-square

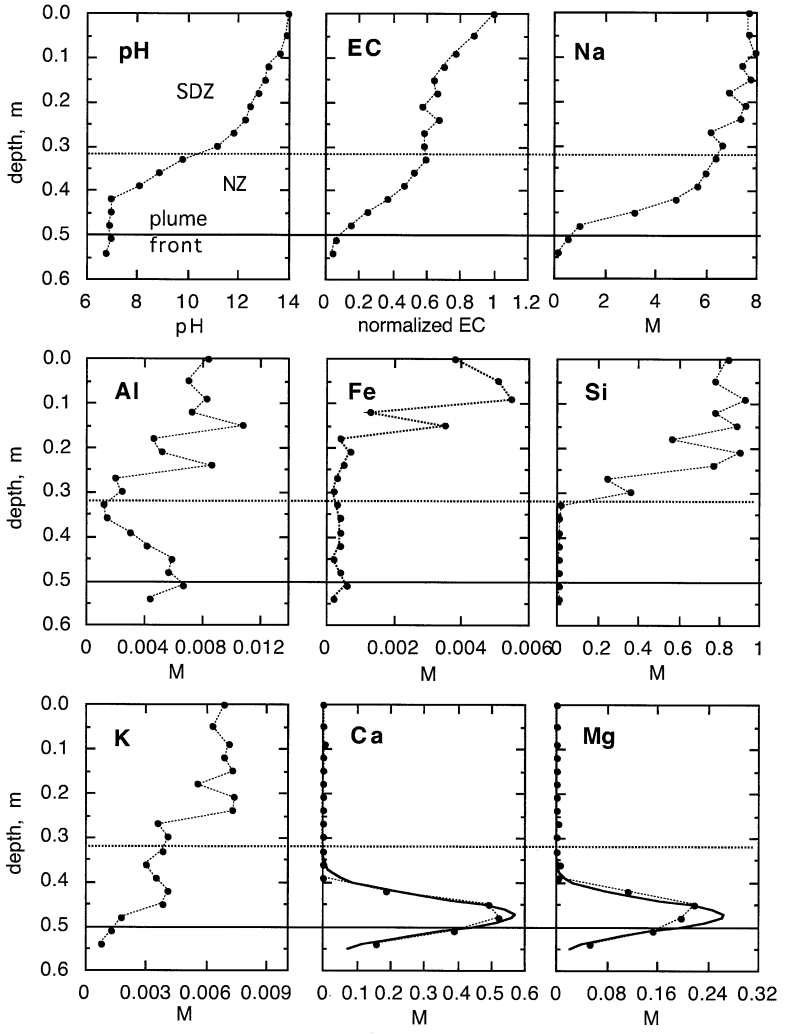

Fig. 6. Pore-water chemical-composition profiles within the 2.0 m column. The experiments were conducted at 70°C, and the waste-plume transport direction is plotted from top down. The smooth curves in the Ca and Mg plots are predications using displacement-dependent dispersion model.

differences was set to 1.5 mm. Fair agreement was obtained between measured and calculated Ca profiles. The same dispersivity was then used for calculations on the Ca^{2+} profile in the 2.0 m column and for the Mg^{2+} profiles in both columns. Solution profiles for Mg^{2+} are similar to those of Ca^{2+}, although less distinct because of its smaller proportion at the exchange sites of the initial sediment. Thus, zones with distinct Ca^{2+} and Mg^{2+} peaks can be useful for locating plume fronts in field borehole profiles.

3.4. Evolution of the Sediment's Elemental Composition

Chemical analyses were also obtained on segments of sediments from which the previously described solution samples were extracted. These profiles of elemental concentrations in the sediments permeated with TWS are presented in Figure 7 (0.6 m column) and Figure 8 (2.0 m column). Individual plots show elemental mass fractions associated with the solid phase. Profiles associated with the combination of solid and aqueous phases are also shown in some plots. The aqueous phase contribution was determined directly from the previously described measured concentrations in suction-collected pore waters. Since the XRF analyses were done on samples that were dried without completely removing aqueous solutions from pores (typically only 20 to 50% of the pore water was extracted in individual samples), the results needed to be corrected by subtraction of contributions from salts deposited from solution during drying. The solid phase concentrations for loss on ignition, Al, Ti, and Fe were simply assigned their respective XRF-determined values, since their aqueous phase inventories were insignificant relative to their respective solids. The solid phase concentrations for Na, Si, K, Ca, and Mg were calculated by subtracting their corresponding remaining aqueous phase masses from XRF values. (Additional curves in Figs. 7 and 8 representing calculated profiles are discussed later.)

Buildup of Na concentrations associated with the solid phase nearest the inlet resulted primarily from precipitation of various Na-bearing solids, and secondarily from cation exchange. The

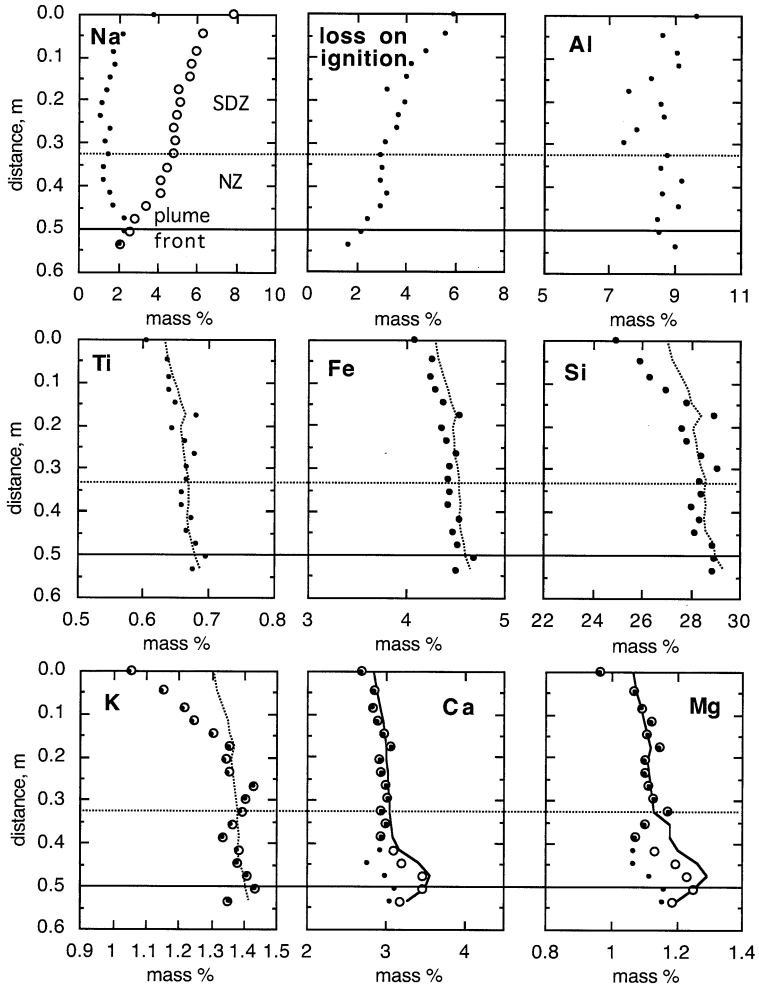

Fig. 7. Elemental composition profiles of the 0.6 m sediment column. Concentrations associated with solid phases are shown in filled circles. Combined solid- and solution-phase concentrations are shown in open circles. Curves represent predictions based on mass dilution, as well as cation exchange, displacement, and dispersion.

precipitating Na-containing solids are initially largely amorphous, and transform into a variety of zeolites, cancrinite, and zeolite-like minerals over time (Wan et al., 2003). Loading of Na^+ onto exchange sites is limited to increases in the range of 0.04 to 0.4 mass percent, based on the previously noted constraints on the cation exchange capacity, and would occur fairly uniformly throughout the TWS-affected region.

The loss on ignition (LOI) profiles include waters of hydration, carbonate-, and nitrate-containing solids. A substantial carbonate-associated component to the LOI values was observed upon reacting sediments with HCl (Fig. 8, LOI profile). The CO_2 manometric procedure (Loeppert and Suarez, 1996) is normally used for estimating calcite concentrations in soils, but is also responsive to a broad range of carbonates, including carbonate cancrinite. The more elevated LOI values nearest the source resulted from these solids precipitating during TWS infiltration into the Hanford sediment. The possibility that Na and LOI solids might have accounted for most of the overall changes in elemental composition of the sediment was tested by using their local concentration changes (relative to the original sediment) to estimate local bulk density increases. These estimated increases in local Na and LOI contents were then used to predict concentration profiles of an essentially nonreacting constituent, Ti, as well as most of the other elements. The profiles of Al within the sediment columns did not exhibit any clear pattern. Since Al is a major component in both the sediment and TWS, the simple mass dilution procedure is not applicable.

The dominant titanium-bearing soil minerals (anatase and rutile) are relatively stable in the sediment. Shown along with the XRF profiles for Ti concentrations are dotted line curves showing the Ti profiles predicted solely from dilution by precipitating the Na and LOI components described previously. The fair agreement between these two profiles indicates that the slightly reduced Ti mass concentrations close to the TWS source are caused by dilution by these other components.

Most of the other elemental profiles shown in Figures 7 and 8 are also expected to exhibit dilution caused by precipitation of new solids. This is evident in the Fe, Si, and K profiles, although the latter two elements have concentrations in the near-source region that are significantly lower than that estimated by simple dilution. Dissolution rates for silicates and

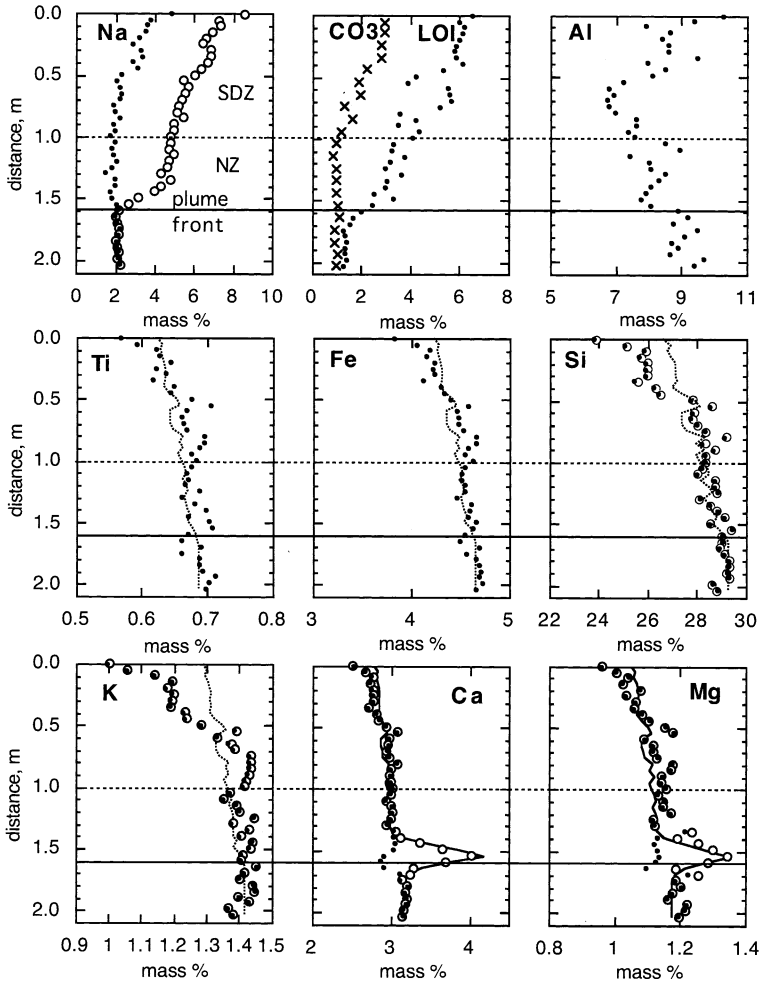

Fig. 8. Elemental composition profiles of the 2 m sediment column. Concentrations associated with solid phases are shown in filled circles. Combined solid- and solution-phase concentrations are shown in open circles. Curves represent predictions based on mass dilution, as well as cation exchange, displacement, and dispersion.

K-feldspar are high under the extremely alkaline conditions existing in the near-source region. Thus, Si and K dissolution and transport are expected to reduce their near-source solid phase concentrations below levels estimated by simple dilution.

The sediment Ca profile reflects the combined influences of displacement by cation exchange with Na, dilution by precipitating Na and LOI solids, and possible dissolution-precipitation of Ca-bearing solids. The previously estimated exchangeable Ca inventory of 49 $mmol_c\ kg^{-1}$ for the original Hanford sediment is equivalent to a mass concentration of 0.10%. Thus, regions within the waste plume are expected to have total Ca concentrations of ~0.1 mass percent less than that of the native soil (region beyond the front). Furthermore, when precipitation of Ca phases is significant, the front should contain a moving Ca mass less than the displaced exchangeable Ca inventory within the plume, and this mobilized Ca should be distributed over a region that grows largely through hydrodynamic dispersion (as previously described). The depleted region within the plume should also exhibit lower total Ca concentrations closer to the TWS inflow source because of dilution from precipitation of Na-containing and LOI solids. The above considerations were combined to obtain the predicted total Ca profiles shown as curves in Figures 7 and 8. Fair agreement was obtained between measured and calculated total Ca profiles.

The profiles for Mg concentrations along the columns are similar to those of Ca, but less developed since the original exchangeable Mg concentration was about six times lower than that of exchangeable Ca. Thus, Mg depletion within the plume region and its accumulation at the front are much less distinct. The Mg profiles were also compared with predictions based on cation exchange, hydrodynamic dispersion, and mass dilution. Again, the predicted profiles are in fair agreement with data.

3.5. Comparison with the Field Borehole Data

In this section, we compare the conceptual model of plume evolution to the geochemical profiles obtained from the slant-borehole samples by the CH2M-HILL Tank Farm Vadose Zone Characterization Project at the SX single-shell tank farm. Tank SX-108 had confirmed leakage starting in 1962, with the estimated leakage volume between 9 and 130 m^3 (Brevick, 1994). The historical major ion composition of SX-108 (presented in

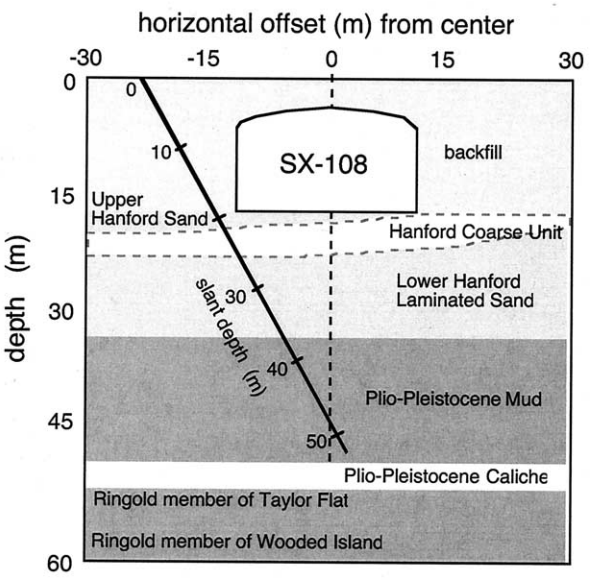

Fig. 9. Cross section of SX-108 Slant Borehole and locations of samples (after Serne et al., 2002b).

Table 1) shows similar but higher salinity and alkalinity than that of the simulated TWS used in our experiments. The SX-108 Slant Borehole (Borehole C3082) samples were collected during June and July of 2000. As illustrated in Figure 9, the borehole was oriented at an angle of ~30° from vertical to obtain samples under the tank. The total length was 52.2 m and vertical depth was 43.9 m (Serne et al., 2002b). Sixteen out of 17 sampling attempts below the tank were successful, with sampling intervals separated from each other by 1.5 to 3.0 m. Because of the low initial moisture content in these field samples, 1:1 (water:sediment) extracts were used to obtain pore-water samples for chemical analyses. Selected analyzed chemical profiles of the water extracts presented in the Slant-Borehole Final Report (Serne et al., 2002b) are shown in Figure 10.

Although the components plotted in Figure 10 are the same as those shown in Figures 5 and 6 from the column experiments, several key differences need to be recognized before comparing the laboratory- and field-based data sets. Differences in source chemistry have been noted above (Table 1). The stratified and heterogeneous nature of the sediments underlying the waste tanks have probably led to complex flow paths for the leaking solutions. Specific locations of the leak source (or sources) and well-constrained estimates on leakage volumes, rates, and duration are not available. In addition to the leaking waste tanks, the field sediments receive periodic natural recharge that will displace and dilute the waste plume. The field samples also collected and analyzed ~40 yr after the leak event and slow kinetic reactions that are not accounted for in the laboratory column tests may be responsible for some of the differences. Finally, the collected core samples constitute a small fraction of below-tank sediment volume, with somewhat sparse coverage even along the length of the borehole.

Despite these differences, the laboratory column experiments provide well-defined signatures of waste-sediment interactions that can help interpret the complex field results. Regions within the subsurface that currently contain the waste plume have elevated salinities and pH. As shown in the column experiments, indicators of mineral dissolution (Fe, Si, and K) are found at higher concentrations within the waste-affected regions. Borehole data appear to intersect two plume fronts, at approximately 32 and 44 m depths below ground surface based on Ca and Mg profiles (Serne et al., 2002b). The laboratory experiments support the use of Ca and Mg for identifying plume boundaries, since their profiles tend to be sharply peaked by rapid and practically complete cation exchange. In the sparsely sampled borehole data set, these two solutes have local maxima consisting essentially of single points. On the other hand, such localized indicators of fronts can easily be missed when sampling intervals are longer than dispersion lengths. Serne et al. (2002b) note that the location of the deeper plume front is ambiguous because concentrations of waste components did not decline to ambient levels in the deepest core samples. The lack of highly elevated pH values in the field core samples may be due to long-term neutralization reactions after cessation of leakage and influxes of atmospheric carbon dioxide or more neutral waters moving down from the backfill.

4. SUMMARY

This study provides a conceptual geochemical model on evolution of saline and alkaline tank waste plumes advancing into underlying sediments. Dramatic pH neutralization of the waste plumes was revealed. The pore water chemistry profiles can be defined as three fairly distinct zones: the silicate dissolution zone (pH $>$ 10), the pH-neutralized zone (pH 10 to 6.5), and displaced native pore waters. The extremely alkaline conditions within the silicate dissolution zone promote dissolution of primary minerals, reflected in elevated concentrations of Si, Fe, and K in pore fluids. The very high Na^+ concentrations in the leaking tank waste solutions drive rapid and complete cation exchange, resulting in highly concentrated levels of Ca^{2+} and Mg^{2+} at the plume front. The quantities of Ca^{2+} and Mg^{2+} in the plume front are within the range expected from cation exchange, and their concentration profiles are represented well by hydrodynamic dispersion. Analyses of the contaminated sediment profiles from the lab tests showed deposition of hydrated solids, carbonates, and nitrate solids. Precipitation of these solids resulted in slight dilution of other elements in the sediment matrix. The net precipitation of solids also decreases the porosity and probably the permeability of the sediment as well. Silicon and potassium exhibited depletion in the silicate dissolution zone beyond that estimated by mass dilution from newly deposited precipitates, as expected based on favorable dissolution kinetics of silicates, feldspars and mica/biotites at very high pH. Most of these laboratory-based findings correspond well to information obtained from a field plume underlying the SX tank farm of the Hanford Site. In addition to the improved basic understanding to the plume-sediment interactions, the results of this study provide a framework useful for interpreting field plume data. Extending this approach of directly simulating and measuring geochemical evolution of waste plumes in laboratory columns to other types of waste plume studies can be beneficial.

Acknowledgments—This work was carried out under U.S. Department of Energy Contract No. DE-AC03-76SF-00098. Funding for the LBL

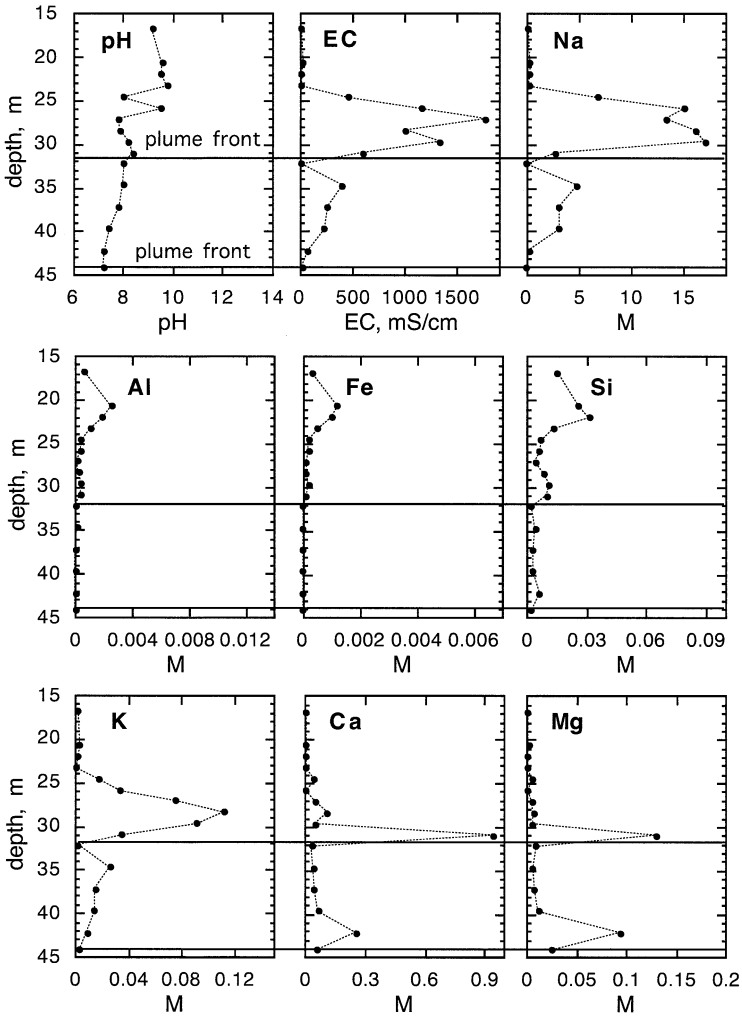

Fig. 10. Chemical composition profiles of pore waters from Well C3082 (SX-108) Slant Borehole sediment samples (after Serne et al., 2002b). The concentrations and EC values were determined on 1:1 water extracts, and then calculated for field moisture contents.

staff was provided by the Environmental Management Science Program while funding for the PNNL staff was provided by CH2M-HILL Hanford Co. The authors thank Rex Couture (Washington University) for XRF analyses of the sediment samples, and Keith Olson (LBNL) for technical support. We also thank the three GCA reviewers and the Associate Editor, George Helz, for their helpful comments.

Associate editor: G. R. Helz

REFERENCES

Agnew S. F., Boyer J., Corbin R. A., Duran T. B., Fitzpatrick J. R., Jurgensen K. A., Ortiz T. P., and Young B. L. (1996) Hanford tank chemical and radionuclide inventories: HDW Model Rev. 3. LA-UR-96-858. Los Alamos National Laboratory.

Bickmore B. R., Nagy K. L., Young J. S., and Drexler J. W. (2001) Nitrate-cancrinite precipitation on quartz sand in simulated Hanford tank solutions. *Environ. Sci. Technol.* **35,** 4481–4486.

Brevick C. H., Gaddis L. A., and Johnson E. D. (1994) Supporting document for the historical tank concent estimate for SX tank farm. WHC-SD-WM-ER-324. Westinghouse Hanford Company.

CH2M HILL Hanford Group. (2001) Site-specific SST phase 1 RFI/CMS work plan addendum for WMAs T and TX-TY, RPP-7578, rev. 1. CH2M HILL Hanford Group.

DOE. (1996) Vadose zone characterization project at the Hanford Tank Farms-SXTank Farm. DOE/ID/12584-268. U.S. Department of Energy.

Hossner L. R. (1996) Dissolution for total elemental analysis. In *Methods of Soil Analysis*, Part 3: *Chemical Methods*, pp. 49–64. (eds. D. L. Sparks, A. L. Page, P. A. Helmke, R. H. Loeppert, P. N. Soltanpour, M. A. Tabatabai, C. T. Johnson, and M. E. Summer), *American Society of Agronomy*, 1996.

Loeppert R. H. and Suarez D. L. (1996) Carbonate and gypsum. In *Methods of Soil Analysis*, Part 3: *Chemical Methods (ed. D. L. Sparks), pp. 437–474. Soil Science Soc. Am.*

Malstrom M. and Banwart S. (1997) Biotite dissolution at 25°C: The pH dependence of dissolution rate and stochiometry. *Geochim. Cosmochim. Acta* **61,** 2779–2799.

McKinley J. P., Zeissler C. J., Zachara J. M., Serne R. J., Lindstrom R. M., Schaef R. T., and Orr R. D. (2001) Distribution and retention of ^{137}Cs in sediments at the Hanford Site, Washington. *Environ. Sci. Technol.* **35,** 3433–3441.

Reidel S. P. and Horton D. G. (1999) Geologic data package for 2001 immobilized low-activity waste performance assessment, PNNL-12257, rev. 1. Pacific Northwest National Laboratory.

Riley R. G., Zachara J. M., Wobber F. J. (1992) Chemical contaminants on DOE lands and selection of contaminant mixtures for subsurface

science research, DOE Office of Energy Research Subsurface Science Program, DOE/ER-0547T. DOE.

Rimstidt J. D. and Barnes H. L. (1980) The kinetics of silica–water reactions. *Geochim. Cosmochim. Acta* **44,** 1683–1699.

Serne R. J., Zachara J. M., and Burke D. S. (1998) Chemical information on tank supernatants, Cs adsorption from tank liquids onto Hanford sediments and field observations of Cs migration from past tank leaks, PNNL-11495. Pacific Northwest National Laboratory.

Serne R. J., LeGore V. L., Last G. V., Schaef H. T., O'Hara M. J., Smith S. C., Bjornstad B. N., Brown C. F., Lindenmeier C. W., Williams B. A., Parker K. E., Zachara J. M, Lanigan D. C., Kutnyakov I. V., Burke D. B., Horton D. G., Serne J. N., Clayton R. E., and Mitroshkov A. V. (2002a) Characterization of uncontaminated sediments from the Hanford Reservation–RCRA borehole core samples and composite samples, PNNL-13757-1. Pacific Northwest National Laboratory.

Serne R. J., Last G. V., Schaef H. T., Lanigan D. C., Lindenmeier C. W., Ainsworth C. C., Clayton R. E., LeGore V. L., O'Hara M. J., Brown C. F., Orr R. D., Kutnyakov I. V., Wilson T. C., Wagnon K. B., Williams B. A. and Burke D.B. (2002b) Geologic and geochemical data and preliminary interpretations of vadose zone sediment from Slant Borehole SX-108 in the S-SX Waste Management Area. PNNL-13757-4. Pacific Northwest National Laboratory.

Swanson L. C., Weeks D. C., Luttrell S. P., Mitchell R. M., Landeen D. S., Johnson A. R., and Roos R. C. (1988) Grout treatment facility environmental baseline and site characterization report, WHC-EP-0150. Westinghouse Hanford Company.

Teng H. H., Fenter P., Cheng L., and Sturchio N. C. (2001) Resolving orthoclase dissolution processes with atomic force microscopy and X-ray reflectivity. *Geochim. Cosmochim. Acta* **65,** 3459–3474.

Wan J., Tokunaga T. K., Saiz E., Larsen J. T., and Olson K. R. (2003) Colloid formation resulted from high salinity and caustic waste tank solution leaking into the underlay sediments at the Hanford site. LBNL-2446. Lawrence Berkeley National Laboratory.

Ward A. L., Gee G. W., and White M. D. (1997) A comprehensive analysis of contaminant transport in the vadose zone beneath tank SX-109, PNNL-11463. Pacific Northwest National Laboratory.

Zachara J. M., Smith S. C., Liu C., McKinley J. P., Serne R. J., and Gassman P. L. (2002) Sorption of Cs^+ to micaceous subsurface sediments from the Hanford site, USA. *Geochim. Cosmochim. Acta* **66,** 193–211.